A Combined Stokes Drift Profile under Swell and Wind Sea

ØYVIND BREIVIK[a]

Norwegian Meteorological Institute, and University of Bergen, Bergen, Norway

KAI H. CHRISTENSEN

Norwegian Meteorological Institute, and University of Oslo, Oslo, Norway

(Manuscript received 28 April 2020, in final form 15 July 2020)

ABSTRACT

A combined directional Stokes drift profile for swell and wind sea is presented. The profile can be used to calculate the shear under crossing seas and as such is relevant for Langmuir turbulence and Stokes–Coriolis forcing, but also for material advection. The swell is represented as either a monochromatic wave or as a Phillips spectrum, while the wind sea is represented as a Phillips spectrum. The profile is found to compare well against the full directional Stokes drift calculated from the 2D spectrum of ERA-Interim in an open-ocean location in the North Atlantic. The error compared to a Phillips-type unidirectional Stokes drift profile is markedly lower for a combined profile with a monochromatic swell Stokes profile. However, representing the swell as a Phillips-type Stokes drift profile yields even better results. The combined profile relies on integrated wave parameters readily available from wave models and can be calculated at low cost. The global Stokes drift climate is investigated using ERA-Interim reanalysis data with the intention of identifying regions dominated by crossing Stokes drift. We find that the eastern equatorial Pacific Ocean probably experiences the greatest degree of crossing Stokes drift, and the entire subtropical band 20°–30°S/N exhibits a significant degree of crossing Stokes drift and swell dominance over the Stokes drift.

KEYWORDS: Wind waves; Langmuir circulation; Mixed layer; Mixing; Atmosphere-ocean interaction; Ocean models

1. Introduction

The Stokes drift (Stokes 1847) is the difference between the Eulerian velocity in a point and the average Lagrangian motion of a water particle undergoing the orbital motion $\mathbf{u}_w$ of a wave field (Longuet-Higgins 1953; Phillips 1977),

$$\mathbf{v}_S = \left\langle \int^t \mathbf{u}_w \, dt' \cdot \nabla \mathbf{u}_w \right\rangle. \tag{1}$$

Here the averaging $\langle \cdot \rangle$ is over a period appropriate for the frequency of surface waves (Phillips 1977; Andrews and McIntyre 1978; Leibovich 1983). Conceptually, this can be written (LeBlond and Mysak 1978; van den Bremer and Breivik 2018) as

$$\underbrace{\mathbf{v}_S}_{\text{Stokes}} = \underbrace{\mathbf{u}_L}_{\text{Lagrange}} - \underbrace{\mathbf{u}_E}_{\text{Euler}}. \tag{2}$$

Stokes drift profiles have commonly been modeled from the assumption of unidirectional, monochromatic waves (see, e.g., Skyllingstad and Denbo 1995; McWilliams et al. 1997; Polton et al. 2005; Saetra et al. 2007). This yields a profile that has too weak shear near the surface and too strong Stokes transport deeper down. The Stokes drift profile under a Phillips-type (Phillips 1958) spectrum was explored by Breivik et al. (2014, hereafter B14), and later in more detail by Breivik et al. (2016, hereafter B16). The Phillips-type Stokes profile was found by B16 to improve both the shear and the transport compared to the earlier, empirical profile proposed by B14. Li et al. (2017) derived an analytical expression for the Stokes transport under the Phillips profile and its depth-averaged profile. The Phillips-type profile was

Denotes content that is immediately available upon publication as open access.

[a] ORCID: 0000-0002-2900-8458.

Corresponding author: Øyvind Breivik, oyvind.breivik@met.no

DOI: 10.1175/JPO-D-20-0087.1

shown to give a good approximation to the profile under an arbitrary spectrum, but it does not address the veering of the profile due to the presence of swell. Here we explore how a Phillips-type Stokes drift profile can be combined with a monochromatic profile or another Phillips-type Stokes drift profile for the swell component, thus providing an efficient way to parameterize a full three-dimensional profile. This has practical implications for the computation of the trajectories of drifting objects (Breivik et al. 2012a,b; Röhrs et al. 2015; Christensen et al. 2018) as well as for the fate of oil in the ocean (McWilliams and Sullivan 2000; Jones et al. 2016; Dagestad et al. 2018) and the drift of eggs and larvae (Röhrs et al. 2014; Strand et al. 2019). It also allows easier experimentation on wave model data to test the potential impact that crossing seas (e.g., swell and wind sea at significant angles to each other) might have on the Stokes production responsible for Langmuir turbulence (Van Roekel et al. 2012; Harcourt 2013; McWilliams et al. 2014; Harcourt 2015; Li et al. 2017; Ali et al. 2019; Breivik et al. 2019). Finally, the Coriolis–Stokes force in coupled models (Fan and Griffies 2014; Breivik et al. 2015; Staneva et al. 2017; Wu et al. 2019a) and the associated Stokes material transport (Wu et al. 2019b) are affected by the shape of the Stokes drift profile. The Stokes drift implementation in ocean models should ideally be based on the Fourier representation of Kenyon (1969), using a linear superposition of the contributions from discrete components of the two-dimensional wave spectrum. With few exceptions (Li et al. 2016), the Stokes drift is approximated based on a unidirectional and monochromatic representation of the wave field (see, e.g., Uchiyama et al. 2010). Implementing a combined swell and broadband wind sea profile as suggested here will allow better control over the Stokes drift profile and its impact on upper-ocean dynamics in realistic ocean models.

Superposition of the Stokes drift of different Fourier components means that, provided we have separated the spectrum into nonoverlapping swell and wind sea parts, we can also decompose the Stokes drift velocity in a swell component (sw) and a wind sea component (ws):

$$\mathbf{v}_S = \mathbf{v}_{\mathrm{sw}} + \mathbf{v}_{\mathrm{ws}}. \tag{3}$$

We are often faced with a situation where we either have access to integrated wave model parameters from one of the main spectral wave models in use today (Hasselmann et al. 1988; Booij et al. 1999; Tolman et al. 2014; ECMWF 2019) or we can make assumptions and construct an idealized wave field (McWilliams et al. 2014). The following discussion assumes that we have access to the integrated parameters significant wave height (H_s), swell and wind sea height (H_{sw}, H_{ws}), mean frequencies ($\overline{\omega}$, $\overline{\omega}_{\mathrm{sw}}$, $\overline{\omega}_{\mathrm{ws}}$) and directions ($\overline{\theta}_{\mathrm{sw}}$, $\overline{\theta}_{\mathrm{ws}}$). In addition, we also have access to (or we dictate) the (total) surface Stokes drift $\mathbf{v}_{S_0}$. Given these (listed in Table 1), we outline how to construct a combined Stokes drift profile for swell and wind sea.

TABLE 1. Integrated parameters required from a wave model (or assumed known) to calculate a combined Stokes drift profile.

Parameter	Variable
Significant wave height	H_s
Swell height	H_{sw}
Wind sea height	H_{ws}
First moment mean frequency	$\overline{\omega}$
First moment swell mean frequency	$\overline{\omega}_{\mathrm{sw}}$
First moment wind sea mean frequency	$\overline{\omega}_{\mathrm{ws}}$
Swell mean direction	$\overline{\theta}_{\mathrm{sw}}$
Wind sea mean direction	$\overline{\theta}_{\mathrm{ws}}$
Surface Stokes drift vector	$\mathbf{v}_{S_0}$

This article is organized as follows. Section 2 explores the degree to which swell and wind sea Stokes drift differ in strength and direction throughout the world's oceans by defining a number of measures of relative Stokes drift and degree of crossing. In section 3 we recapitulate the properties of the Stokes drift profile and remind the reader of the features of a Phillips-type spectrum and its associated Stokes drift profile. In section 4 we derive the combined profile for a monochromatic swell component and a wideband wind sea spectrum for which we assume the Phillips profile. We also consider using a Phillips type spectrum for the swell. In section 5 we compare the combined profile against the Stokes drift profile calculated from the full two-dimensional (2D) spectrum of the ERA-Interim (Dee et al. 2011) wave model. Finally, section 6 discusses the practical use of such a combined profile and where in the world's oceans the competing influence of swell and wind sea affects the Stokes drift profile the most.

2. Global swell and wind sea Stokes drift climate

For a directional wave variance density spectrum $E(\omega, \theta)$ ($\mathrm{m^2\,s\,rad^{-2}}$), the Stokes drift velocity in deep water is given by

$$\mathbf{v}_S(z) = \frac{2}{g}\int_0^{2\pi}\int_0^{\infty} \omega^3 \hat{\boldsymbol{\theta}} e^{2kz} E(\omega, \theta)\, d\omega\, d\theta, \tag{4}$$

where ω is the circular frequency, z the vertical coordinate (positive up, and negative below sea level) and $\hat{\boldsymbol{\theta}}$ the unit vector in the direction of wave propagation θ. This can be derived from the expression for a wavenumber spectrum in arbitrary depth (Kenyon 1969), using the deep-water dispersion relation $\omega^2 = gk$ (with $g \approx 9.81\,\mathrm{m\,s^{-2}}$ the acceleration due to gravity). The circular frequency spectrum is defined as

$$F(\omega) \equiv \int_0^{2\pi} E(\omega, \theta)\, d\theta,$$

for which the Stokes drift speed profile becomes

$$v_S(z) = \frac{2}{g}\int_0^{\infty} \omega^3 e^{2kz} F(\omega)\, d\omega. \tag{5}$$

From Eq. (5) it is clear that at the surface the Stokes drift is proportional to the third spectral moment [where the nth spectral moment of the circular frequency is defined as $m_n = \int_0^{\infty} \omega^n F(\omega)\, d\omega$],

$$v_{S_0} = 2m_3/g. \tag{6}$$

While Eq. (5) yields the Stokes drift speed at different depths, the direction of the two-dimensional velocity vector, Eq. (4), can vary significantly, as the degree to which swell and wind sea directions deviate varies greatly throughout the world's oceans. The extratropics exhibit a mix of local wind sea and swell (Semedo et al. 2011, 2015) whereas the swell-dominated tropics are mostly unaffected by wind sea. To quantify the relative impact of the swell and the wind sea and the degree of misalignment we now define and investigate a number of quantities.

a. The Stokes balancing depth D_b

The first quantity we consider is the Stokes balancing depth D_b at which the swell and wind sea Stokes drift speed are equal in strength, found by solving the following equation for z:

$$\left|\mathbf{v}_{\mathrm{sw}}(z)\right| = \left|\mathbf{v}_{\mathrm{ws}}(z)\right|. \tag{7}$$

The Stokes balancing depth is here used to investigate the regional differences in swell and wind sea contributions to the total Stokes drift. For this specific part of the analysis, the wind sea and the swell parts will each be represented by a monochromatic profile,

$$v_m(z) = v_0 e^{2kz}. \tag{8}$$

Using a monochromatic profile will yield a slightly larger balancing depth than if we employ a more complex parametric profile because it decays more slowly (B16). This is acceptable as it is the relative geographical differences that we wish to investigate, and those will remain the same. At $z = -D_b$ we then have

$$v_{\mathrm{sw}_0} e^{-2k_{\mathrm{sw}}D_b} = v_{\mathrm{ws}_0} e^{-2k_{\mathrm{ws}}D_b}. \tag{9}$$

Here, v_{sw_0} and v_{ws_0} are the surface Stokes drift speed of the swell and wind sea part of the wave spectrum, respectively.

The monochromatic swell wavenumber can be found from the linear deep-water dispersion relation,

$$k_{\mathrm{sw}} = \omega_{\mathrm{sw}}^2/g. \tag{10}$$

The swell Stokes transport is proportional to the first spectral moment of the swell spectrum (using the circular frequency ω), m_1^{sw}, and can thus be calculated from the swell height and mean frequency (B14),

$$V_{\mathrm{sw}} = m_1^{\mathrm{sw}} = \overline{\omega}_{\mathrm{sw}} H_{\mathrm{sw}}^2/16. \tag{11}$$

The monochromatic surface swell Stokes drift speed can then be found as

$$v_{\mathrm{sw}_0} = 2k_{\mathrm{sw}} V_{\mathrm{sw}}. \tag{12}$$

The same procedure gives us the monochromatic wind sea surface Stokes drift and wavenumber, with all swell quantities in Eqs. (10)–(12) replaced by their wind sea counterparts. These are readily available from wave models. For the mean frequencies, we have used the first moment, $\overline{\omega} = m_1/m_0$, but this is of minor importance when comparing geographical differences.

The balancing depth can now be found,

$$D_b = \frac{\ln\left(v_{\mathrm{ws}_0}/v_{\mathrm{sw}_0}\right)}{2\left(k_{\mathrm{ws}} - k_{\mathrm{sw}}\right)}. \tag{13}$$

Figure 1 shows the Stokes balancing depth for ERA-Interim, averaged over the years 2010–12, inclusively. Note that we set all cases where $D_b < 0$ to zero to reduce the effect of cases where there is no solution [i.e., where the swell height is smaller than the wind sea height and $\ln(v_{\mathrm{ws}_0}/v_{\mathrm{sw}_0}) < 0$]. The windy extratropics have very large balancing depths, which is unsurprising as the extratropical weather systems generate wind sea that on average is much stronger than the swell. We have capped the color scale at 20 m as we are primarily interested in subtropical and tropical regions where the swell Stokes drift is comparable in strength to the wind sea Stokes drift. The two cells north and south of equator in the Pacific Ocean correspond to regions where the trade winds blow steadily. This leads to a relatively large balancing depth. By comparison, the region from the Galápagos Islands toward Central America exhibits a very shallow balancing depth. This is explained by the weak winds near the equator. The swell on the other hand remains almost unchanged. This leads the swell Stokes drift to dominate over the wind sea Stokes drift, which shows up as a shallow balancing depth. The seasonal variation of the balancing depth is explored in the appendix. We see there that the most important feature

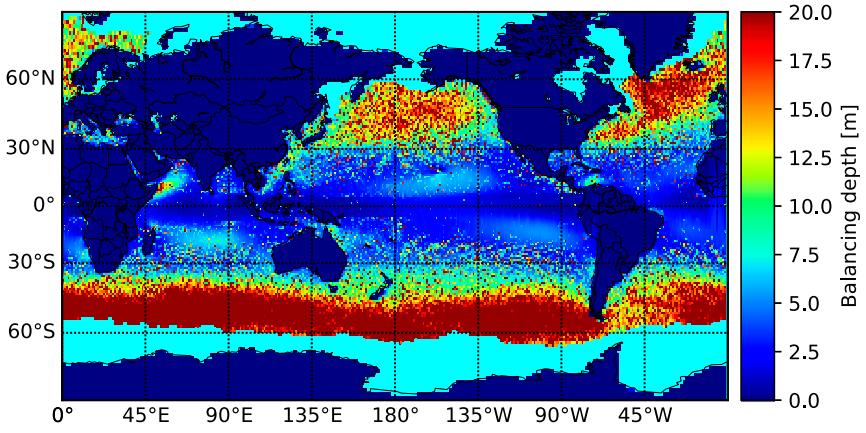

FIG. 1. The average balancing depth of swell and wind sea Stokes drift (m) for ERA-Interim for the years 2010–12 (0000, 0600, 1200, and 1800 UTC).

is a strengthening of the degree of crossing in the northern equatorial and subtropical band from 0° to 30°N in the northern winter.

b. *The Stokes depth ratio*

A simpler estimate of the relative importance of the swell is the swell to wind sea Stokes *e*-folding depth ratio (not to be confused with the balancing depth D_b),

$$r_D = \frac{D_{\mathrm{sw}}}{D_{\mathrm{ws}}} = \frac{V_{\mathrm{sw}}/v_{\mathrm{sw}_0}}{V_{\mathrm{ws}}/v_{\mathrm{ws}_0}}. \tag{14}$$

Here, the Stokes transport is defined as $V = \int_{-\infty}^{0} v_S \, dz$. Again the subscripts refer to the swell and wind sea part of the spectrum. Since $D_{\mathrm{ws}} = 1/2k_{\mathrm{ws}}$ and $D_{\mathrm{sw}} = 1/2k_{\mathrm{sw}}$, we can write this simply as

$$r_D = k_{\mathrm{ws}}/k_{\mathrm{sw}}. \tag{15}$$

Figure 2 shows the ratio of the swell Stokes depth to the wind sea Stokes depth. We see that the areas where the swell Stokes *e*-folding depth is unusually large compared to the wind sea Stokes depth coincide with the regions where the balancing depth (Fig. 1) is large. It is also interesting to note that the depth ratio remains large in a larger region in the equatorial Pacific than what is found for the balancing depth (see the region between 180° and 135°W, south of the equator). In regions where the wind sea Stokes *e*-folding depth is shallow compared to the swell counterpart, i.e., where $k_{\mathrm{ws}} \gg k_{\mathrm{sw}}$, the balancing depth approaches

$$\lim_{k_{\mathrm{ws}}/k_{\mathrm{sw}} \to \infty} D_b = \frac{\ln\left(v_{\mathrm{ws}_0}/v_{\mathrm{sw}_0}\right)}{2k_{\mathrm{ws}}},$$

which is independent of k_{sw}. This could mean that a decrease in the balancing depth D_b while r_D stays more

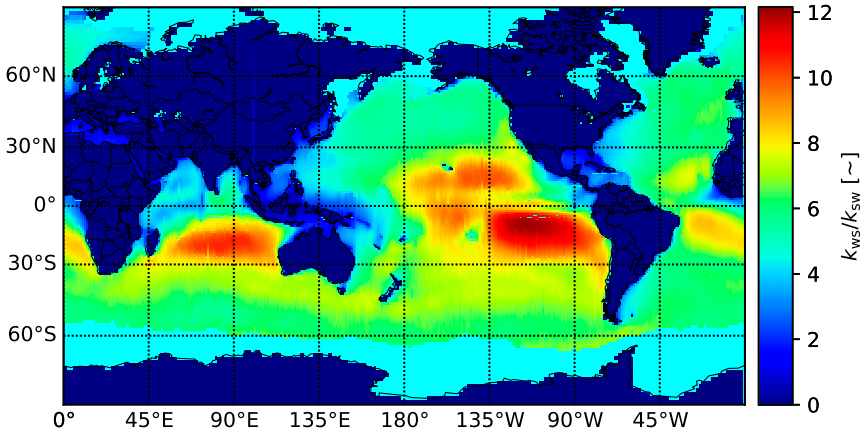

FIG. 2. The average *e*-folding depth ratio of swell over wind sea Stokes drift for ERA-Interim for the years 2010–12 (0000, 0600, 1200, and 1800 UTC).

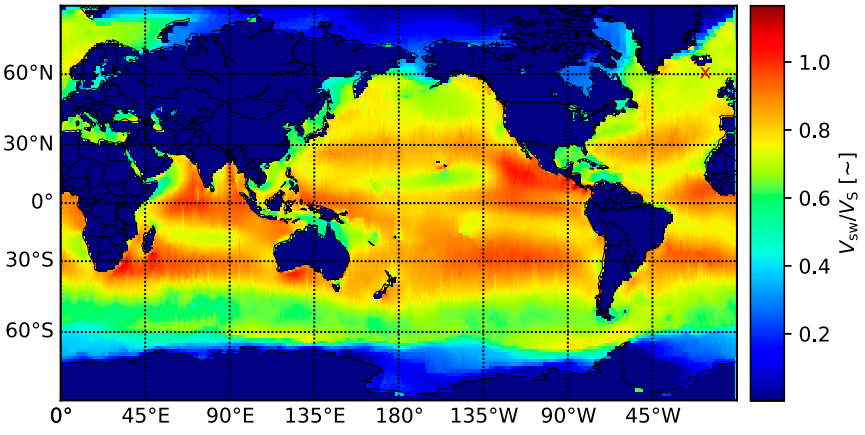

FIG. 3. The average ratio of swell over total Stokes transport for ERA-Interim for the years 2010–12 (0000, 0600, 1200, and 1800 UTC). The location used for comparison with the full 2D ERA-Interim spectra, 60°N, 340°E in the North Atlantic (just south of Iceland) is indicated by the "X".

or less the same could be caused by a decrease in the ratio v_{ws_0}/v_{sw_0} or by an increase in k_{ws}.

c. Stokes swell transport ratio

The third quantity that can shed light on the importance of the swell Stokes drift is the ratio of the swell Stokes transport to the total transport,

$$r_V = V_{sw}/V_S. \tag{16}$$

Figure 3 shows the degree to which the swell Stokes transport dominates the tropics. The reason the ratio of swell to total transport sometimes exceeds unity is that the total transport is reduced by directional spread, whereas the swell transport is calculated on the assumption of unidirectional waves, see the discussion in section 4 and Eq. (11). It is clear that the swell transport totally dominates the tropics and the subtropical regions outside the trade wind belts (Carrasco et al. 2014; Breivik et al. 2019). As expected, the swell transport ratio drops rapidly outside the latitude belt ±40°. The extratropics, and in particular the Southern Ocean, exhibits swell transport ratios around 50%. This is quite in line with what is known about the wave climate in general (Aarnes et al. 2017; Morim et al. 2019) and the swell climate in particular (Semedo et al. 2011, 2015).

d. Degree of crossing Stokes drift

Finally, the degree to which swell and wind sea directions diverge can be used as a proxy for how much the effect of crossing seas should affect the Langmuir turbulence (Belcher et al. 2012; Van Roekel et al. 2012; McWilliams et al. 2014) in the turbulent kinetic energy (TKE) equation,

$$\frac{De}{Dt} = \underbrace{-\overline{\mathbf{u}_H'w'}\cdot\frac{\partial \mathbf{u}_H}{\partial z}}_{1} \underbrace{-\overline{\mathbf{u}_H'w'}\cdot\frac{\partial \mathbf{v}_S}{\partial z}}_{2\text{—Stokes prod}} + \underbrace{\overline{w'b'}}_{3} \underbrace{-\frac{\partial}{\partial z}\left(\overline{w'u_i'u_i'} + \frac{1}{\rho_w}\overline{w'p'}\right)}_{4} - \underbrace{\varepsilon}_{5}. \tag{17}$$

Here we have followed the notation used by Belcher et al. (2012); $e = \overline{u_i'u_i'}/2$ represents the turbulent kinetic energy per unit mass. The shear production term (1) involves the shear of the horizontal mean Eulerian flow $\mathbf{u}_H$. Primes indicate turbulent quantities, with w' the vertical component. The Stokes production term (2) of interest here is similar in form to the Eulerian shear production but involves instead the shear of the Stokes drift. The buoyancy term (3) depends on the turbulent buoyancy fluctuations b'. Term 4 represents the turbulent transport and pressure correlation terms (Stull 1988; Kantha and Clayson 2000). Finally, term 5, ε, is the TKE dissipation term.

By defining the degree of crossing as

$$r_\times = \hat{\mathbf{z}}\cdot\frac{\mathbf{v}_{ws_0}\times\mathbf{v}_{sw_0}}{\left|\mathbf{v}_{S_0}\right|^2} = \frac{v_{ws_0}v_{sw_0}}{v_{S_0}^2}\sin\left(\theta_{ws}-\theta_{sw}\right) \tag{18}$$

we get a dimensionless number $r_\times \in [-1/2, 1/2]$ that depends on the ratio of the cross product of the swell and wind sea over the total surface Stokes drift. Here, $\hat{\mathbf{z}}$ is the vertical unit vector (upward). As we have defined it here, the degree of crossing is positive when the wind sea is to the right of the swell. Both the relative strength and the angle between the swell and the wind sea affect the degree of crossing. The maximum absolute value (1/2) is

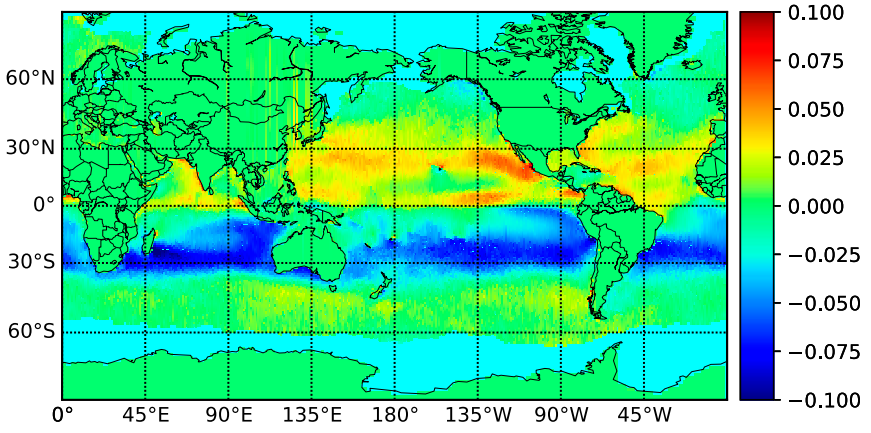

FIG. 4. The average normalized degree of crossing of swell and wind sea surface Stokes drift for ERA-Interim for the years 2010–12 (0000, 0600, 1200, and 1800 UTC). Positive values indicate that the wind sea Stokes drift is to the right of the swell.

attained for swell and wind sea of equal strength at right angles. Figure 4 shows that the degree of crossing is quite substantial in the deep tropics, but negligible in the extratropics (where the directional differences between swell and wind sea tend to average out with the passing of low pressure systems). This is as expected, but highlights the importance of swell in the tropics. It is interesting to note that the sign changes at the equator, with wind sea being to the left of the swell south of the equator. This is explained mainly by the swell propagating from the Southern Ocean, but also by the general direction of the trade winds. The whole band from 20° to 30°S shows a strong degree of crossing Stokes drift. This is also the case, although to a lesser degree, for the northern subtropics, 20°–30°N. The seasonal variation is investigated in the appendix, where it is seen that the most important difference is a strengthening of the degree of crossing in the subtropical and equatorial Northern Hemisphere in the northern summer.

3. Properties of the Phillips profile

The Phillips spectrum (Phillips 1958)

$$F_{\text{Phil}} = \begin{cases} \alpha g^2 \omega^{-5}, & \omega > \omega_p \\ 0, & \omega \le \omega_p \end{cases}, \tag{19}$$

yields a reasonable estimate of the part of the spectrum which contributes most to the Stokes drift velocity near the surface, i.e., the high-frequency waves. Here ω_p is the peak frequency. We assume Phillips' parameter $\alpha = 0.0083$. The Stokes drift velocity profile under (19) is

$$v_{\text{Phil}}(z) = 2\alpha g \int_{\omega_p}^{\infty} \omega^{-2} e^{2\omega^2 z/g}\, d\omega. \tag{20}$$

An analytical solution exists for (20); see B14, their Eq. (11). Using the deep-water dispersion relation, Eq. (20) can be written as

$$v_{\text{Phil}}(z) = \frac{2\alpha g}{\omega_p}\left[e^{-2k_p|z|} - \sqrt{2\pi k_p|z|}\,\text{erfc}\left(\sqrt{2k_p|z|}\right)\right]. \tag{21}$$

Here erfc is the complementary error function and $k_p = \omega_p^2/g$ is the peak wavenumber. From Eq. (21) we see that for the Phillips spectrum, Eq. (20), the surface Stokes drift velocity is $2\alpha g/\omega_p$.

Let us assume (B16) that the Phillips spectrum profile (21) is a reasonable approximation for Stokes drift velocity profiles under a general spectrum,

$$v_S(z) \approx v_{S_0}\left[e^{-2\overline{k}|z|} - \beta\sqrt{2\pi\overline{k}|z|}\,\text{erfc}\left(\sqrt{2\overline{k}|z|}\right)\right], \tag{22}$$

where β is a parameter. The profile differs from the monochromatic profile, Eq. (8), in the added error function term, which makes the shear stronger near the surface and the deep Stokes drift weaker. The total Stokes transport under Eq. (22) can be found (see appendix A of B16) to be

$$V = \frac{v_0}{2\overline{k}}(1 - 2\beta/3). \tag{23}$$

We can now determine the inverse depth scale $\overline{k}$, given an estimate of the transport V and the surface Stokes drift velocity v_0. Both, as B14 argued, are normally available from wave models. Note that we still need to estimate β, but B16 found $\beta = 1$ to yield good agreement between modeled and parameterized Stokes drift profiles. In the following we will exclusively use this value.

Note also that estimating the Stokes transport from a one-dimensional Stokes drift profile will overestimate it since the directional spreading of waves tends to cancel out some of the contributions. This effect is ignored by assuming all waves to be propagating in the same direction. The Stokes transport from a unidirectional profile should typically be reduced by about 17% (Ardhuin et al. 2009; B14). The spreading factor proposed by Webb and Fox-Kemper (2015) could be used to further correct the profile.

a. *The layer average of the Stokes drift profile under the Phillips spectrum*

Li et al. (2017) found a closed-form expression for the integral of Eq. (22), i.e., the Stokes drift transport between the vertical level z_0 and the surface,

$$V(z_0) = \frac{v_0}{2\overline{k}}\left\{1 - e^{-2\overline{k}|z_0|} - \frac{2\beta}{3}\left[1 + \sqrt{\pi}\left(2\overline{k}|z_0|\right)^{3/2} \times \mathrm{erfc}\left(\sqrt{2\overline{k}|z_0|}\right) - \left(1 + 2\overline{k}|z_0|\right)e^{-2\overline{k}|z_0|}\right]\right\}. \tag{24}$$

See their appendix A for a full derivation. To find the average Stokes drift between a lower-level z_0 and an upper-level z_1 all that is needed is to use Eq. (24) twice to find

$$\overline{v}_S(z_0, z_1) = \frac{V(z_0) - V(z_1)}{z_1 - z_0}. \tag{25}$$

Here we have indicated that the chosen vertical range affects the averaging by writing $\overline{v}_S(z_0, z_1)$. This simple method for calculating the layer-averaged Phillips Stokes drift in the expression makes it convenient for calculation of the layer-averaged Langmuir number (Harcourt and D'Asaro 2008),

$$\mathrm{La}_{\mathrm{SL}} = \frac{u_*}{\overline{v}_S - v_S(z_{\mathrm{ref}})},$$

where u_* is the oceanside friction velocity and z_{ref} is a reference depth.

b. *The shear under the Phillips profile*

The shear under Eq. (22) is straightforward to find (B16),

$$\frac{\partial v_S}{\partial z} = v_{S_0}\left[2(1-\beta)\overline{k}e^{-2\overline{k}|z|} + \beta\sqrt{\frac{\pi\overline{k}}{2|z|}}\,\mathrm{erfc}\left(\sqrt{2\overline{k}|z|}\right)\right], \tag{26}$$

which simplifies to

$$\frac{\partial v_S}{\partial z} = v_{S_0}\sqrt{\frac{\pi\overline{k}}{2|z|}}\,\mathrm{erfc}\left(\sqrt{2\overline{k}|z|}\right), \tag{27}$$

when $\beta = 1$. The latter (27) is of course particularly convenient and can readily be used to analytically calculate related quantities like the depth-averaged weighted Stokes drift shear (Kukulka and Harcourt 2017).

4. A combined Stokes drift profile for swell and wind sea

We will in the following impose the constraint (3) that the wind sea surface Stokes drift is determined as

$$\mathbf{v}_{\mathrm{ws}_0} = \mathbf{v}_{S_0} - \mathbf{v}_{\mathrm{sw}_0}. \tag{28}$$

This total surface Stokes drift is assumed to be found with a wave model or otherwise decided by the experimenter [see, e.g., McWilliams et al. (2014), who constructed a combined profile by dictating the wind sea and swell strength and direction]. There are no strong compelling reasons for determining the wind sea Stokes drift strength and direction from the swell and the total sea other than the fact that the swell direction is often more precisely known from climatology. We could thus equally well have chosen to determine the swell from the wind sea and the total Stokes drift.

a. *A monochromatic swell profile*

Let us first assume that the swell is well represented by the monochromatic profile such that

$$\mathbf{v}_{\mathrm{sw}} = v_{\mathrm{sw}_0}e^{2k_{\mathrm{sw}}z}\hat{\boldsymbol{\theta}}_{\mathrm{sw}}. \tag{29}$$

Here $\hat{\boldsymbol{\theta}}_{\mathrm{sw}} = (\sin\theta_{\mathrm{sw}}, \cos\theta_{\mathrm{sw}})$ is a unit vector in the swell propagation direction (oceanographic convention, i.e., measured as going to and clockwise from north). We can now derive the surface wind sea Stokes drift from Eq. (28),

$$\mathbf{v}_{\mathrm{ws}_0} = \mathbf{v}_{S_0} - v_{\mathrm{sw}_0}\hat{\boldsymbol{\theta}}_{\mathrm{sw}}.$$

b. *Imposing swell and wind sea direction*

The procedure above will lead to a wind sea Stokes drift that is not necessarily in the direction of the wind sea as it is dictated by the swell surface Stokes drift, which in turn is estimated from the assumption that the swell is monochromatic. In a real wave model, this is not the case, and the swell direction and strength will be composed of several Fourier components in the 2D spectrum. This may still work well in idealized cases (McWilliams et al. 2014), but is not desirable when we

have access to model output of wind sea and swell directions. It is however possible to add the constraint that both the swell and the wind sea Stokes drift surface vectors are in line with the swell ($\theta_{\rm sw}$) and wind sea ($\theta_{\rm ws}$) direction. Our constraint (28) says that the surface Stokes drift must be preserved,

$$\mathbf{v}_{S_0} = \upsilon_{{\rm ws}_0}\hat{\boldsymbol{\theta}}_{\rm ws} + \upsilon_{{\rm sw}_0}\hat{\boldsymbol{\theta}}_{\rm sw}. \tag{30}$$

We can then work out the speed of the swell surface Stokes drift by taking the cross product of Eq. (30) and $\hat{\boldsymbol{\theta}}_{\rm ws}$,

$$\mathbf{v}_{S_0} \times \hat{\boldsymbol{\theta}}_{\rm ws} = \upsilon_{{\rm sw}_0}\hat{\boldsymbol{\theta}}_{\rm sw} \times \hat{\boldsymbol{\theta}}_{\rm ws}.$$

This yields the following relation,

$$\upsilon_{{\rm sw}_0} = \frac{\upsilon_E\hat{\theta}_N^{\rm ws} - \upsilon_N\hat{\theta}_E^{\rm ws}}{\hat{\theta}_E^{\rm sw}\hat{\theta}_N^{\rm ws} - \hat{\theta}_N^{\rm sw}\hat{\theta}_E^{\rm ws}}. \tag{31}$$

Here, $(\hat{\theta}_E^{\rm ws}, \hat{\theta}_N^{\rm ws}) = \hat{\boldsymbol{\theta}}_{\rm ws}$ and $(\hat{\theta}_E^{\rm sw}, \hat{\theta}_N^{\rm sw}) = \hat{\boldsymbol{\theta}}_{\rm sw}$ are components of the unit vectors in the direction of the wind sea and swell, respectively. Finally, $(\upsilon_E, \upsilon_N) = \mathbf{v}_{S_0}$ are the components of the total surface Stokes drift vector. Finally, the wind sea Stokes drift is found from Eq. (30). Note that Eq. (31) is ill conditioned and will often lead to negative values due to round off errors, particularly if the swell and wind sea components point in the same or the opposite direction. In practice, we therefore also calculate $\upsilon_{{\rm ws}_0}$ according to the same procedure and choose the one that is nonnegative.

We now have enough information to estimate the swell and wind sea wavenumbers, either from Eq. (12) for the monochromatic or Eq. (23) for the Phillips Stokes drift profile [where we find $V_{\rm sw}$ from Eq. (11) and $V_{\rm ws}$ is computed in the same manner using corresponding wind sea quantities]. In the following analysis we use this method to determine the direction of the wind sea Stokes drift profile.

c. A Phillips wind sea profile

Assume that Eq. (22) is a good approximation for the wind sea part of the Stokes drift profile, and let the surface Stokes drift from the wind sea part of the spectrum be defined as

$$\upsilon_{{\rm ws}_0} = \left|\mathbf{v}_{S_0} - \mathbf{v}_{{\rm sw}_0}\right|. \tag{32}$$

This constraint, see Eq. (28), forces the sum of the swell and wind sea surface Stokes drift to sum to the total surface Stokes drift. The wind sea transport $V_{\rm ws}$ is determined similarly as the swell transport, Eq. (11),

$$V_{\rm ws} = m_1^{\rm ws} = \overline{\omega}_{\rm ws}H_{\rm ws}^2/16, \tag{33}$$

Finally, the inverse depth scale (or wavenumber) of the wind sea profile is found from Eq. (23),

$$k_{\rm ws} = \frac{\upsilon_{{\rm ws}_0}}{2V_{\rm ws}}(1 - 2\beta/3). \tag{34}$$

To ensure that the surface Stokes drift vector is preserved, the direction of the wind sea profile should be determined from Eq. (3), $\hat{\boldsymbol{\theta}}_{\rm ws} = (\mathbf{v}_{S_0} - \mathbf{v}_{{\rm sw}_0})/\upsilon_{{\rm ws}_0}$. Note that the transport under the combined profile will be smaller or equal to the transport under the one-dimensional profile resulting from the total sea state parameters since the swell and wind sea components will partially cancel each other out unless they are in perfect alignment (see the discussion by B14).

This procedure allows us to estimate a combined profile with a directional veering due to the presence of swell. The parameters can all be estimated from standard output from atmosphere–wave reanalyses such as ERA-Interim (Dee et al. 2011) or regional wave hindcasts like NORA10 (Reistad et al. 2011; Haakenstad et al. 2020).

d. Two Phillips profiles

As an alternative to the assumption that swell is well represented by a monochromatic profile, we can instead assume two Phillips profiles, one for the swell part and one for the wind sea part of the spectrum. This has the added complication that since we now assume a broad-banded spectrum (the Phillips spectrum) for the swell, we can no longer calculate the wavenumber from the swell peak frequency through the dispersion relation (10). However, following the procedure (31)–(34) and by computing the transports according to Eq. (11) allows us to calculate both the monochromatic and Phillips wavenumbers with equal ease.

5. Comparison against ERA-Interim 2D Stokes drift profiles

Following the same procedure as B14 and B16, we here compare the full 2D Stokes drift profile calculated from the ERA-Interim (Dee et al. 2011) reanalysis against three profiles. The first is a Phillips profile, identical to that explored by B16, in the direction of the surface Stokes drift. The second profile is a combined monochromatic swell and Phillips wind sea profile, and the third is a combination of two Phillips profiles, one for the swell component and one for the wind sea. A full year of spectra from location 60°N, 340°W at 0000 UTC is used (location indicated in Fig. 3). The location is characterized by a mixture of swell and wind sea (Semedo et al. 2011) and is thus well suited for investigating the

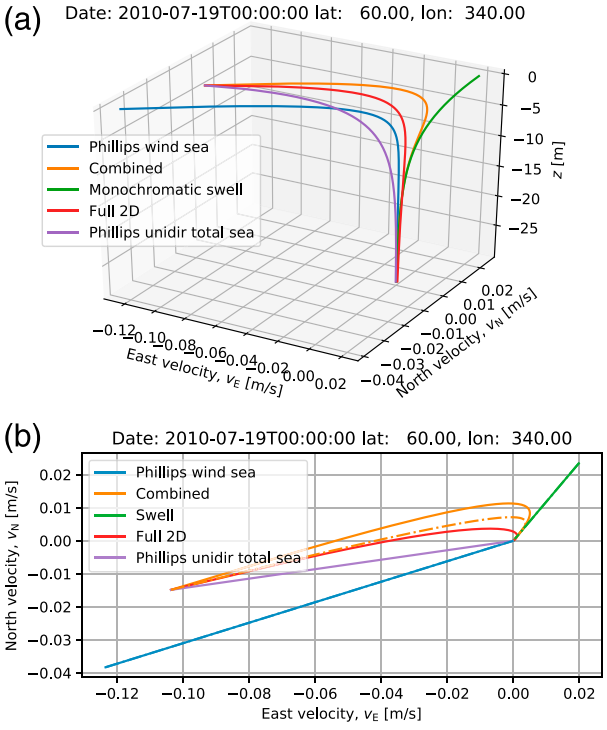

FIG. 5. (a) A perspective view of a monochromatic swell Stokes profile (green) and Phillips wind sea (blue) yielding a combined profile (orange) that matches the full 2D ERA-Interim profile (red) much better than the unidirectional Phillips Stokes profile (purple). (b) A bird's eye view. Here, a Phillips swell profile is also shown (dashed). It is seen to compare even better than the monochromatic profile.

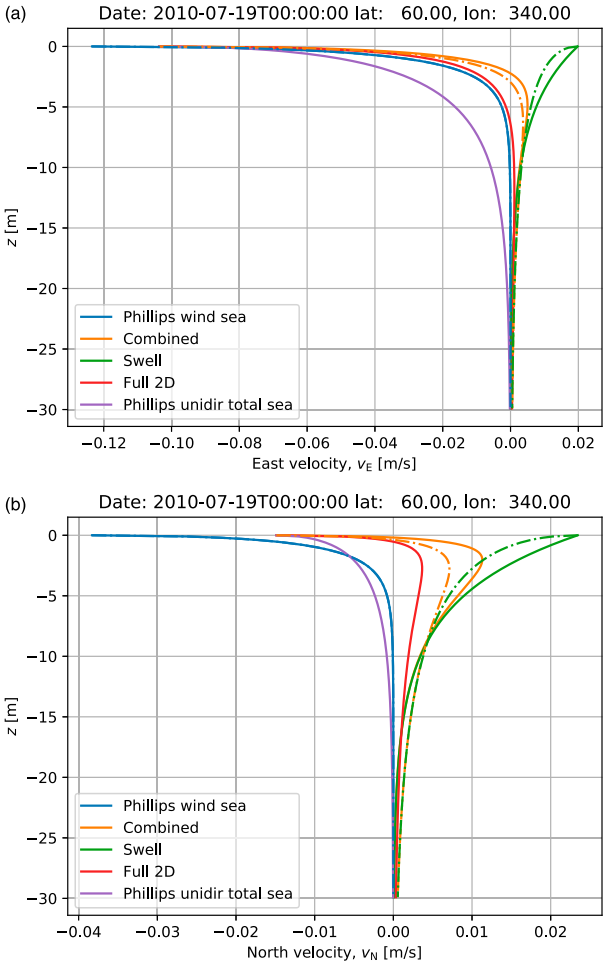

FIG. 6. The (a) east and (b) north component vertical profiles of the profile presented in Fig. 5. The Phillips swell profile (green dashed) yields a total profile (orange dashed) that comes closer to the full profile (red).

performance of the combined Stokes drift profile. It also coincides with the location used by B14 and B16 (as does the choice of ERA-Interim spectra for the year 2010). The ERA-Interim data used are the same as those used for the global statistics in section 2. The 2D spectra used for the calculation of the full Stokes drift profile have a directional resolution of 15° and cover the frequency range 0.0345–0.548 Hz with logarithmic spacing. The spatial resolution of the wave model component of ERA-Interim is approximately 110 km. We compute the 2D Stokes drift velocity vector at every 10 cm from the surface down to 30-m depth from the full spectra.

To illustrate the performance of the combined profiles, derived from the integrated parameters listed in Table 1, we start by choosing a rather demanding case where we have swell going in the northeast direction and wind sea propagating nearly diametrically in the west-southwest direction. Figures 5 and 6 give a 3D perspective and a 2D bird's eye view of the Stokes drift profiles for the given situation, respectively. A short explanation to the figures is justified. First, the monochromatic swell profile is drawn in green in Fig. 5a. It can be seen to point almost diametrically opposite to the Phillips wind sea profile (blue). They combine to form the orange curve, which should be compared to the red curve that represents the full profile, calculated from the ERA-Interim 2D wave spectrum. For comparison we also include the unidirectional Phillips profile (purple). We see that the combined profile does a fairly good job at representing the total profile, and it is certainly an improvement over the Phillips unidirectional profile. Moving to the bird's eye view (Fig. 5b), we see that the veering of the full profile is captured, but overdone (orange, fully drawn curve), by the combined monochromatic (swell, green) and Phillips (wind sea, blue) Stokes drift profile (Fig. 5a). This is improved significantly by exchanging the monochromatic swell profile with a Phillips-type profile (orange, dashed curve). This may seem surprising as we would expect the swell to be

quite monochromatic. It is however important to keep in mind that real swell is not monochromatic, and we are after all trying to model a full 2D spectrum with a somewhat arbitrary separation of swell and wind sea performed by the wave model itself [see the discussion by ECMWF (2019), Breivik et al. (2019), and Strand et al. (2019) about the swell separation algorithm and its consequences for the swell statistics]. Figure 6 shows that the east and north components of the Stokes drift profile confirm the impression that representing the swell with a Phillips-type Stokes profile (dashed green curve) seems to do a better job than the monochromatic profile (green fully drawn curve). The total profile (orange dashed) is much closer to the red curve representing the total profile than the combination of a monochromatic swell profile with a Phillips wind sea Stokes profile.

In Figs. 7a–c we assess for the year 2010, like B16 did, the departure of the combined profiles from the full profile by calculating the normalized absolute difference as

$$\delta V = V^{-1}\int_{-30\mathrm{m}}^{0} |v_{\mathrm{mod}} - v|\, dz\,. \tag{35}$$

Here v represents the Stokes drift speed of the full 2D Stokes drift profile of the wave model and the Stokes transport $V = \int_{-\infty}^{0} v\, dz$. It is evident that the Phillips unidirectional profile (Fig. 7a) has a higher normalized error than the combined Phillips wind sea and monochromatic swell profile (Fig. 7b), about 23%. However, using two Phillips Stokes profiles (as outlined above) representing wind sea and swell reduces the normalized mean error further (a total reduction of about 37%).

The reduction of (the nonnormalized) transport magnitude error,

$$\Delta V = \int_{-30\mathrm{m}}^{0} |v_{\mathrm{mod}} - v|\, dz\,. \tag{36}$$

is shown in Figs. 7d–f. This is an estimate of the departures in Stokes drift speed at each vertical level. As we can see, the speed is evidently much better represented by the combined profiles (Figs. 7e,f) than by the unidirectional profile (Fig. 7d).

The (nonnormalized) east and north components of the transport error are calculated as

$$\Delta V_i = \int_{-30\mathrm{m}}^{0} (v_{\mathrm{mod},i} - v_i)\, dz. \tag{37}$$

Here v_i represents either east or north components of the Stokes drift vector. These are shown in Fig. 8. The reduction in error in directional components is quite significant, and as for the normalized transport error, the component-wise error reduction is considerably greater for the combined Phillips Stokes profiles (about 40% reduction, and about 25% reduction for the combined monochromatic swell and Phillips wind sea Stokes profiles). Figures 7d–f and 8 together demonstrate that the combined profiles reduce errors in both the speed and the directional components of the Stokes drift, and, importantly, that combining two Phillips Stokes profiles reduces the error more than using a monochromatic profile for the swell component.

6. Discussion and concluding remarks

The combined profile is shown to reduce the overall error by about a third compared to a unidirectional Phillips profile in a location with mixed swell and wind sea conditions in the North Atlantic Ocean (60°N, 340°E, see Fig. 3). This is significant and it is thus a convenient alternative to calculating the full 2D profile from a wave model. We find significant differences between the Phillips and a monochromatic swell Stokes profile, and recommend using a combination of two Phillips Stokes profile.

The question of how such a combined profile will affect ocean models that rely on Stokes drift profiles for Langmuir turbulence and Coriolis–Stokes forcing can only be answered by running dedicated model experiments. It is still clear that the added degrees of freedom that the profile admits will allow much more complex Stokes drift profiles to be explored. This should allow easier experimentation on the question of whether crossing seas really do weaken the Langmuir turbulence (Van Roekel et al. 2012; McWilliams et al. 2014; Ali et al. 2019).

The global Stokes drift climate has been investigated using ERA-Interim reanalysis data. Two new quantities, the degree of crossing [Eq. (4)] and the Stokes drift balancing depth, i.e., the depth below which the swell Stokes drift is stronger than the wind sea Stokes drift [Eq. (13)], suggest that the region west of Central America exhibits a combination of strong swell at large angles to the local wind sea. The bands along 20°–30°S and to a smaller extent along 20°–30°N exhibit a high degree of crossing and can be expected to be very dominated by the large directional spread between the wind sea and the swell Stokes drift. We conclude that the degree of crossing is a useful quantity for identifying regions with significant deviation in the swell and wind sea Stokes drift direction. It is not enough to simply look at the deviation in wind sea and swell wave propagation direction, since the swell Stokes drift is in many cases so much weaker than the wind sea Stokes drift to be

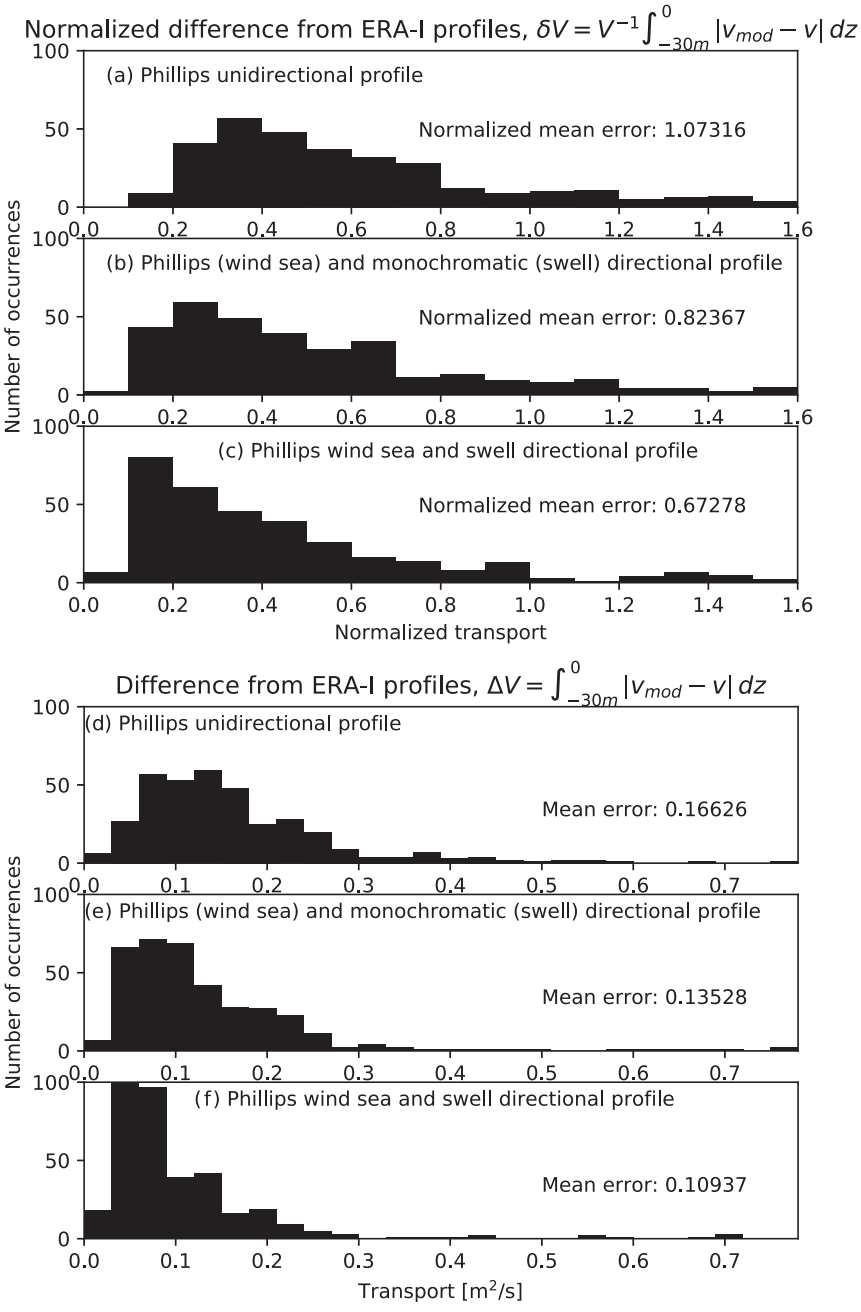

FIG. 7. Histogram of the (a)–(c) normalized and (d)–(f) nonnormalized deviation between the magnitude of the full 2D profile and the 1D Phillips profile in (a) and (d), the 2D combined monochromatic swell and Phillips wind sea profile in (b) and (e), and two Phillips profiles in (c) and (f). The profile is integrated between $z = -30$ m and the surface. ERA-Interim spectra for the year 2010 (0000 and 1200 UTC) in the location 60°N, 340°E in the North Atlantic are used.

negligible. The balancing depth is also found to yield valuable information, but we note that it becomes noisy in the extratropics, something we attribute to the dominance of wind sea over swell. It is suited for the equatorial and subtropical regions where it clearly highlights regions where the balancing depth is small (i.e., where the strength of the swell Stokes drift rapidly overtakes the wind sea Stokes drift with depth). Further studies of the potential impact of crossing seas on Langmuir turbulence and the Stokes–Coriolis force demand ocean

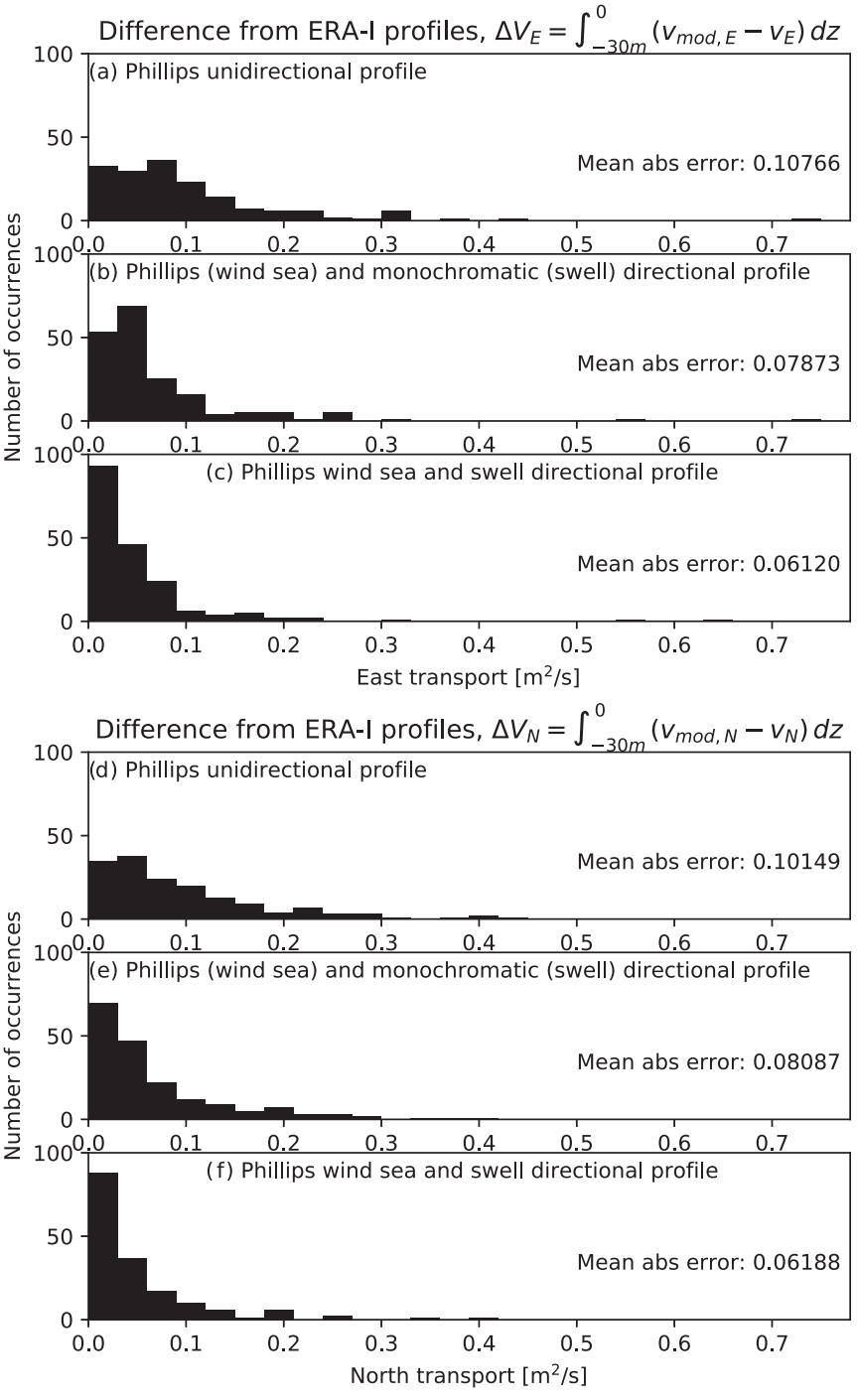

FIG. 8. Histogram of the (nonnormalized) deviation between the (a)–(c) east and (d)–(f) north components of the full 2D profile and the 1D Phillips profile in (a) and (d), the 2D combined monochromatic swell and Phillips wind sea profile in (b) and (e), and two Phillips profiles in (c) and (f). The profile is integrated between $z = -30$ m and the surface. ERA-Interim spectra for the year 2010 (0000 and 1200 UTC) in location 60°N, 340°E in the North Atlantic are used.

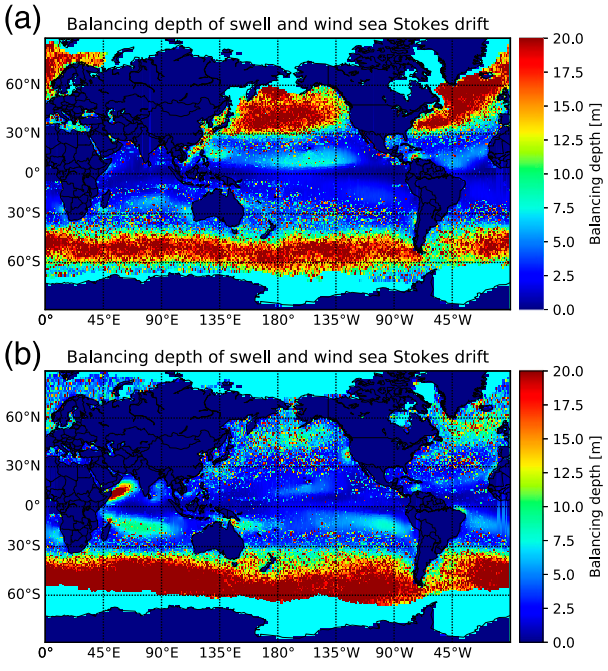

FIG. A1. The seasonally averaged balancing depth of swell and wind sea Stokes drift (m) for ERA-Interim for the years 2010–12 (0000, 0600, 1200, and 1800 UTC) for (a) January–March and (b) July–September.

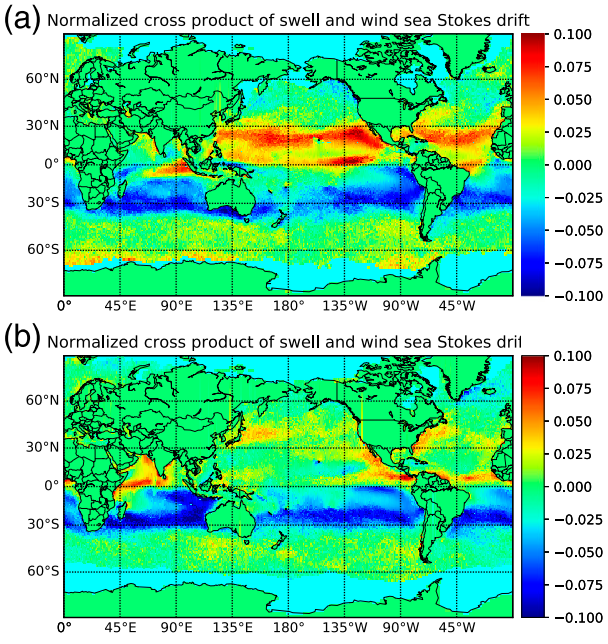

FIG. A2. The seasonally averaged normalized degree of crossing of swell and wind sea surface Stokes drift for ERA-Interim for the years 2010–12 (0000, 0600, 1200, and 1800 UTC) for (a) January–March and (b) July–September. Positive values indicate that the wind sea Stokes drift is to the right of the swell.

models that either take into account the Stokes drift profile from the full 2D spectrum of a wave model, or a combined parameterized Stokes drift profile as outlined in section 4.

Acknowledgments. We gratefully acknowledge support from the Research Council of Norway through the CIRFA project (Grant 237906) as well as the Copernicus Marine Environmental Monitoring Service (CMEMS) and Mercator Ocean through the WaveFlow Service Evolution project. We would also like to thank the two anonymous reviewers who with their comments made the paper a much better one. The data used are available through the ECMWF MARS archive. All parameters can be found with a standard request (experiment ID 1), except the Stokes drift which must be fetched from experiment FJVC.

APPENDIX

Seasonal Variation in Global Stokes Drift Parameters

The seasonal variation in swell and wind sea wave climate leads to significant changes in the seasonal Stokes drift climate. Figure A1 shows the seasonal impact on the balancing depth (see Fig. 1). The balancing depth shows a clear seasonal variation in the Indian Ocean, where the southwestern monsoon increases the Stokes drift balancing depth in the northern summer (less dominated by swell Stokes drift). In the northern subtropical Pacific Ocean the balancing depth is clearly reduced (becoming more dominated by swell Stokes drift) in the northern summer.

Figure A2 shows that the degree of crossing (see also Fig. 4) remains quite unchanged in the southern equatorial and subtropical band from 0° to 30°S, whereas the northern equatorial and subtropical band from 0° to 30°N shows a large degree of seasonal variation in the degree of crossing throughout all three ocean basins with much more crossing Stokes drift in the northern winter.

REFERENCES

Aarnes, O. J., and Coauthors, 2017: Projected changes in significant wave height towards the end of the 21st century: Northeast Atlantic. *J. Geophys. Res. Oceans*, **122**, 3394–3403, https://doi.org/10.1002/2016JC012521.

Ali, A., K. Christensen, Ø. Breivik, M. Malila, R. Raj, L. Bertino, E. Chassignet, and M. Bakhoday-Paskyabi, 2019: A comparison of Langmuir turbulence parameterizations and key wave effects in a numerical model of the North Atlantic and Arctic Oceans. *Ocean Modell.*, **137**, 76–97, https://doi.org/10.1016/j.ocemod.2019.02.005.

Andrews, D. G., and M. E. McIntyre, 1978: An exact theory of nonlinear waves on a Lagrangian-mean flow. *J. Fluid Mech.*, **89**, 609–646, https://doi.org/10.1017/S0022112078002773.

Ardhuin, F., L. Marié, N. Rascle, P. Forget, and A. Roland, 2009: Observation and estimation of Lagrangian, Stokes, and Eulerian currents induced by wind and waves at the sea surface. *J. Phys. Oceanogr.*, **39**, 2820–2838, https://doi.org/10.1175/2009JPO4169.1.

Belcher, S. E., and Coauthors, 2012: A global perspective on Langmuir turbulence in the ocean surface boundary layer. *Geophys. Res. Lett.*, **39**, L18605, https://doi.org/10.1029/2012GL052932.

Booij, N., R. C. Ris, and L. H. Holthuijsen, 1999: A third-generation wave model for coastal regions 1. Model description and validation. *J. Geophys. Res.*, **104**, 7649–7666, https://doi.org/10.1029/98JC02622.

Breivik, Ø., A. Allen, C. Maisondieu, J.-C. Roth, and B. Forest, 2012a: The leeway of shipping containers at different immersion levels. *Ocean Dyn.*, **62**, 741–752, https://doi.org/10.1007/s10236-012-0522-z.

——, T. C. Bekkvik, A. Ommundsen, and C. Wettre, 2012b: BAKTRAK: Backtracking drifting objects using an iterative algorithm with a forward trajectory model. *Ocean Dyn.*, **62**, 239–252, https://doi.org/10.1007/s10236-011-0496-2.

——, P. Janssen, and J. Bidlot, 2014: Approximate Stokes drift profiles in deep water. *J. Phys. Oceanogr.*, **44**, 2433–2445, https://doi.org/10.1175/JPO-D-14-0020.1.

——, K. Mogensen, J.-R. Bidlot, M. A. Balmaseda, and P. A. Janssen, 2015: Surface wave effects in the NEMO ocean model: Forced and coupled experiments. *J. Geophys. Res. Oceans*, **120**, 2973–2992, https://doi.org/10.1002/2014JC010565.

——, J.-R. Bidlot, and P. A. Janssen, 2016: A Stokes drift approximation based on the Phillips spectrum. *Ocean Modell.*, **100**, 49–56, https://doi.org/10.1016/j.ocemod.2016.01.005.

——, A. Carrasco, J. Staneva, A. Behrens, A. Semedo, J.-R. Bidlot, and O. J. Aarnes, 2019: Global Stokes drift climate under the RCP8.5 scenario. *J. Climate*, **32**, 1677–1691, https://doi.org/10.1175/JCLI-D-18-0435.1.

Carrasco, A., A. Semedo, P. E. Isachsen, K. H. Christensen, and Ø. Saetra, 2014: Global surface wave drift climate from ERA-40: The contributions from wind-sea and swell. *Ocean Dyn.*, **64**, 1815–1829, https://doi.org/10.1007/s10236-014-0783-9.

Christensen, K., Ø. Breivik, K.-F. Dagestad, J. Röhrs, and B. Ward, 2018: Short-term predictions of oceanic drift. *Oceanography*, **31**, 59–67, https://doi.org/10.5670/oceanog.2018.310.

Dagestad, K.-F., J. Röhrs, Ø. Breivik, and B. Ådlandsvik, 2018: OpenDrift v1.0: A generic framework for trajectory modeling. *Geosci. Model Dev.*, **11**, 1405–1420, https://doi.org/10.5194/gmd-11-1405-2018.

Dee, D. P., and Coauthors, 2011: The ERA-Interim reanalysis: Configuration and performance of the data assimilation system. *Quart. J. Roy. Meteor. Soc.*, **137**, 553–597, https://doi.org/10.1002/qj.828.

ECMWF, 2019: IFS Documentation CY43r1, Part VII: ECMWF Wave Model. Tech. Rep., 99 pp., https://www.ecmwf.int/en/elibrary/19311-part-vii-ecmwf-wave-model.

Fan, Y., and S. M. Griffies, 2014: Impacts of parameterized Langmuir turbulence and non-breaking wave mixing in global climate simulations. *J. Climate*, **27**, 4752–4775, https://doi.org/10.1175/JCLI-D-13-00583.1.

Haakenstad, H., Ø. Breivik, M. Reistad, and O. J. Aarnes, 2020: NORA10EI: A revised regional atmosphere-wave hindcast for the North Sea, the Norwegian Sea and the Barents Sea. *Int. J. Climatol.*, **40**, 4347–4373, https://doi.org/10.1002/joc.6458.

Harcourt, R., 2013: A second-moment closure model of Langmuir turbulence. *J. Phys. Oceanogr.*, **43**, 673–697, https://doi.org/10.1175/JPO-D-12-0105.1.

——, 2015: An improved second-moment closure model of Langmuir turbulence. *J. Phys. Oceanogr.*, **45**, 84–103, https://doi.org/10.1175/JPO-D-14-0046.1.

Harcourt, R. R., and E. A. D'Asaro, 2008: Large-eddy simulation of Langmuir turbulence in pure wind seas. *J. Phys. Oceanogr.*, **38**, 1542–1562, https://doi.org/10.1175/2007JPO3842.1.

Hasselmann, S., and Coauthors, 1988: The WAM model—A third generation ocean wave prediction model. *J. Phys. Oceanogr.*, **18**, 1775–1810, https://doi.org/10.1175/1520-0485(1988)018<1775:TWMTGO>2.0.CO;2.

Jones, C. E., and Coauthors, 2016: Measurement and modeling of oil slick transport. *J. Geophys. Res. Oceans*, **121**, 7759–7775, https://doi.org/10.1002/2016JC012113.

Kantha, L. H., and C. A. Clayson, 2000: *Small Scale Processes in Geophysical Fluid Flows*. International Geophysics Series, Vol. 67, Academic Press, 883 pp.

Kenyon, K. E., 1969: Stokes drift for random gravity waves. *J. Geophys. Res.*, **74**, 6991–6994, https://doi.org/10.1029/JC074i028p06991.

Kukulka, T., and R. R. Harcourt, 2017: Influence of Stokes drift decay scale on Langmuir turbulence. *J. Phys. Oceanogr.*, **47**, 1637–1656, https://doi.org/10.1175/JPO-D-16-0244.1.

LeBlond, P. H., and L. A. Mysak, 1978: *Waves in the Ocean*. Elsevier, 602 pp.

Leibovich, S., 1983: The form and dynamics of Langmuir circulations. *Annu. Rev. Fluid Mech.*, **15**, 391–427, https://doi.org/10.1146/annurev.fl.15.010183.002135.

Li, Q., A. Webb, B. Fox-Kemper, A. Craig, G. Danabasoglu, W. G. Large, and M. Vertenstein, 2016: Langmuir mixing effects on global climate: WAVEWATCH III in CESM. *Ocean Modell.*, **103**, 145–160, https://doi.org/10.1016/j.ocemod.2015.07.020.

——, B. Fox-Kemper, Ø. Breivik, and A. Webb, 2017: Statistical models of global Langmuir mixing. *Ocean Modell.*, **113**, 95–114, https://doi.org/10.1016/j.ocemod.2017.03.016.

Longuet-Higgins, M. S., 1953: Mass transport in water waves. *Philos. Trans. Roy. Soc. London*, **245A**, 535–581, https://doi.org/10.1098/rsta.1953.0006.

McWilliams, J. C., P. Sullivan, and C.-H. Moeng, 1997: Langmuir turbulence in the ocean. *J. Fluid Mech.*, **334**, 1–30, https://doi.org/10.1017/S0022112096004375.

——, and P. P. Sullivan, 2000: Vertical mixing by Langmuir circulations. *Spill Sci. Technol. Bull.*, **6**, 225–237, https://doi.org/10.1016/S1353-2561(01)00041-X.

——, E. Huckle, J. Liang, and P. Sullivan, 2014: Langmuir turbulence in swell. *J. Phys. Oceanogr.*, **44**, 870–890, https://doi.org/10.1175/JPO-D-13-0122.1.

Morim, J., and Coauthors, 2019: Robustness and uncertainties in global multivariate wind-wave climate projections. *Nat. Climate Change*, **9**, 711–718, https://doi.org/10.1038/s41558-019-0542-5.

Phillips, O. M., 1958: The equilibrium range in the spectrum of wind-generated waves. *J. Fluid Mech.*, **4**, 426–434, https://doi.org/10.1017/S0022112058000550.

——, 1977: *The Dynamics of the Upper Ocean*. 2nd ed. Cambridge University Press, 336 pp.

Polton, J. A., D. M. Lewis, and S. E. Belcher, 2005: The role of wave-induced Coriolis-Stokes forcing on the wind-driven mixed layer. *J. Phys. Oceanogr.*, **35**, 444–457, https://doi.org/10.1175/JPO2701.1.

Reistad, M., Ø. Breivik, H. Haakenstad, O. J. Aarnes, B. R. Furevik, and J.-R. Bidlot, 2011: A high-resolution hindcast of wind and waves for the North Sea, the Norwegian Sea, and the Barents Sea. *J. Geophys. Res.*, **116**, C05019, https://doi.org/10.1029/2010JC006402.

Röhrs, J., K. H. Christensen, F. Vikebø, S. Sundby, Ø. Saetra, and G. Broström, 2014: Wave-induced transport and vertical mixing of pelagic eggs and larvae. *Limnol. Oceanogr.*, **59**, 1213–1227, https://doi.org/10.4319/lo.2014.59.4.1213.

——, A. Sperrevik, K. Christensen, Ø. Breivik, and G. Broström, 2015: Comparison of HF radar measurements with Eulerian and Lagrangian surface currents. *Ocean Dyn.*, **65**, 679–690, https://doi.org/10.1007/s10236-015-0828-8.

Saetra, Ø., J. Albretsen, and P. Janssen, 2007: Sea-state-dependent momentum fluxes for ocean modeling. *J. Phys. Oceanogr.*, **37**, 2714–2725, https://doi.org/10.1175/2007JPO3582.1.

Semedo, A., K. Sušelj, A. Rutgersson, and A. Sterl, 2011: A global view on the wind sea and swell climate and variability from ERA-40. *J. Climate*, **24**, 1461–1479, https://doi.org/10.1175/2010JCLI3718.1.

——, R. Vettor, Ø. Breivik, A. Sterl, M. Reistad, C. G. Soares, and D. C. A. Lima, 2015: The wind sea and swell waves climate in the Nordic seas. *Ocean Dyn.*, **65**, 223–240, https://doi.org/10.1007/s10236-014-0788-4.

Skyllingstad, E. D., and D. W. Denbo, 1995: An ocean large-eddy simulation of Langmuir circulations and convection in the surface mixed layer. *J. Geophys. Res.*, **100**, 8501–8522, https://doi.org/10.1029/94JC03202.

Staneva, J., V. Alari, Ø. Breivik, J.-R. Bidlot, and K. Mogensen, 2017: Effects of wave-induced forcing on a circulation model of the North Sea. *Ocean Dyn.*, **67**, 81–101, https://doi.org/10.1007/s10236-016-1009-0.

Stokes, G. G., 1847: On the theory of oscillatory waves. *Trans. Cambridge Philos. Soc.*, **8**, 441–455.

Strand, K., F. Vikebø, S. Sundby, A. Sperrevik, and Ø. Breivik, 2019: Sub-surface maxima in buoyant fish eggs indicate vertical velocity shear and spatially limited spawning grounds. *Limnol. Oceanogr.*, **64**, 1239–1251, https://doi.org/10.1002/lno.11109.

Stull, R. B., 1988: *An Introduction to Boundary Layer Meteorology*. Kluwer Academic, 666 pp.

Tolman, H. L., and Coauthors, 2014: User manual and system documentation of WAVEWATCH III TM version 4.18. Tech. Rep. 276, MMAB/NCEP/NOAA, 311 pp.

Uchiyama, Y., J. C. McWilliams, and A. F. Shchepetkin, 2010: Wave–current interaction in an oceanic circulation model with a vortex-force formalism: Application to the surf zone. *Ocean Modell.*, **34**, 16–35, https://doi.org/10.1016/j.ocemod.2010.04.002.

van den Bremer, T., and Ø. Breivik, 2018: Stokes drift. *Philos. Trans. Roy. Soc.*, **376A**, 20170104, https://doi.org/10.1098/RSTA.2017.0104.

Van Roekel, L. P., B. Fox-Kemper, P. P. Sullivan, P. E. Hamlington, and S. R. Haney, 2012: The form and orientation of Langmuir cells for misaligned winds and waves. *J. Geophys. Res.*, **117**, C05001, https://doi.org/10.1145/2335755.2335816.

Webb, A., and B. Fox-Kemper, 2015: Impacts of wave spreading and multidirectional waves on estimating Stokes drift. *Ocean Modell.*, **96**, 49–64, https://doi.org/10.1016/j.ocemod.2014.12.007.

Wu, L., A. Rutgersson, and Ø. Breivik, 2019a: Ocean-wave-atmosphere interaction processes in a fully coupled modelling system. *J. Adv. Model. Earth Syst.*, **11**, 3852–3874, https://doi.org/10.1029/2019MS001761.

——, J. Staneva, Ø. Breivik, A. Rutgersson, A. G. Nurser, E. Clementi, and G. Madec, 2019b: Wave effects on coastal upwelling and water level. *Ocean Modell.*, **140**, 101405, https://doi.org/10.1016/j.ocemod.2019.101405.